Petroleum Science 23 (2026) 1519–1532

Contents lists available at ScienceDirect

Petroleum Science

journal homepage: www.keaipublishing.com/en/journals/petroleum-science

Original Paper

Study on the sealing performance of the K-type metal sealing ring of the subsea Christmas tree

Yu-Fang Li [a,b,c], Shi-Bin Ye [c], Ying-Ying Wang [a,b,*], Ze-Qing Lin [a,b], Nan Li [d], Bao-Fu Wang [e]

[a] Hainan Institute of China University of Petroleum (Beijing), Sanya, 572024, Hainan, China
[b] College of Safety and Ocean Engineering, China University of Petroleum (Beijing), Beijing, 102249, China
[c] School of Mechanical and Electrical Engineering, Wuhan Institute of Technology, Wuhan, 430205, Hubei, China
[d] Offshore Oil Engineering Co., Ltd, Tianjin, 300461, China
[e] Engineering Technology Branch of CNOOC Energy Development Co., Ltd, Tianjin, 300450, China

ARTICLE INFO

Article history:
Received 8 May 2025
Received in revised form
18 September 2025
Accepted 23 November 2025
Available online 3 December 2025

Edited by Teng Zhu and Min Li

Keywords:
Deep-sea oil and gas development
Subsea Christmas tree
Tubing hanger
K-type metal sealing ring
Sealing contact stress
Precompression amount

ABSTRACT

The Christmas tree tubing hanger serves as a channel for oil, gas, and electrical flow, supporting the tubing string and sealing the annular space. The sealing performance of the tubing hanger is important for ensuring the safe operation of the subsea Christmas tree. The effect of precompression load on the performance of the K-type metal seal was simulated and analyzed through two-dimensional and three-dimensional contact models, and the impact of oil and gas operating pressures, temperatures, and the elastic modulus on the sealing performance of the K-type metal seal was investigated. According to the results, the maximum error between the theoretical calculation and the finite element method for the contact stress on the exterior of the K-type metal seal was 4.72%. The contact stress of the sealing ring increased at higher precompression and internal pressure. Temperature had a minimal impact on the sealing performance of the seal, while reducing the elastic modulus of the sealing ring decreased its equivalent stress. Finally, static pressure and pressure cycling tests were conducted in compliance with the API 6A standard. The tests confirmed that the maximum sealing pressure of the K-type metal seal satisfied the requirement of a 1.5-fold working pressure and validated that the seal exhibited good sealing performance in oil and gas pressure-temperature cycling conditions. The K-type metal seal was self-tightening, where the pressure enhanced the sealing effect, Hertz contact theory can be used for preliminary parameter design in the early stage, and the sealing performance can be further verified through elastic-plastic finite element method and experiments.

1. Introduction

Subsea production systems are crucial for the development of deepwater oil and gas fields, representing vital infrastructure for the offshore exploitation of these resources (Jiao et al., 2024; Yang et al., 2023a, 2023b). The subsea Christmas tree is connected to the underwater wellhead and external transmission pipeline to control the flow and pressure of oil and gas (Meng et al., 2024; Mi et al., 2023; Pang et al., 2024). The tubing hanger is a key component that connects the subsea Christmas tree to the downhole production string. Its main functions include suspending the tubing string, sealing the annular space between the tubing string and the Christmas tree or the casing string, and providing a passage for production well fluids (Chen et al., 2020; Wang et al., 2022b). The tubing hanger mainly consists of a drive ring, a shrink ring, an upper body, a K-type metal sealing ring, a guide sleeve, a locking ring, a body, an annular sleeve, a guide mandrel, a guide block, and other components. Since the tubing hanger and tubing string are situated in the main production passage of the subsea Christmas tree, their failure significantly impacts the overall reliability of the system (Pang et al., 2021; Saithala et al., 2021). The horizontal section of the tubing hanger contains an oil outlet, which serves as the passage for oil flow. Two K-type metal sealing rings are positioned on both the upper and lower sides of the outlet to seal the annular radial gap. The performance

* Corresponding author.
E-mail address: wyy5186@126.com (Y.-Y. Wang).
Peer review under the responsibility of China University of Petroleum (Beijing).

https://doi.org/10.1016/j.petsci.2025.11.044

of these sealing rings is crucial for safe subsea oil and gas extraction. Seal failure can cause severe marine environmental pollution, making effective sealing essential (Li et al., 2023a; Liu et al., 2024). As the challenges of subsea oil development escalate, the tubing hanger system requires enhanced technology, including higher sealing pressure ratings, sealing materials resistant to acidic environments, and adequate sealing performance in varying temperature conditions (An et al., 2022; Jiao et al., 2024; Li et al., 2023b). Since several countries have implemented patent protection and technological barriers for tubing hanger sealing technology, the sealing rings utilized in domestic offshore oil development are primarily imported. Therefore, research on annular K-type metal seals for tubing hangers is crucial for advancing subsea Christmas tree sealing technology and for localizing related metal seal components.

Based on API 17D and ASME VIII-1 standards, Luo et al. (2014) established a calculation model for tubing hangers that considers design pressure and thermal stress, and proposed a design method for horizontal Christmas tree tubing hangers. Xie et al. (2025) conducted a sensitivity analysis on the sealing performance of K-shaped metal seals using a multi factor analysis method, the results showed that the external contact width, inner lip width, and groove radius were the main design variables affecting the sealing performance. Current studies, both domestically and abroad, mainly utilize finite element simulation to assess the effect of parameters such as precompression, operational fluid temperature, pressure, and structure on the equivalent stress and contact stress distribution of uniquely shaped metal sealing rings in different working conditions. The precompression load directly affects the contact performance. Appropriate compression can effectively enhance the contact stress of the sealing element. However, insufficient compression may cause initial sealing failure, while excessive precompression can crush the sealing ring. Therefore, reasonable compression control is vital to ensure effective metal seal performance (Qin et al., 2017). Zhang et al. (2015) used finite element method to analyze the effects of interference fit, pressure, and temperature on the maximum Mises stress and maximum contact stress of K-shaped metal seals, the results showed that the maximum Mises stress and maximum contact stress increased with the interference fit, working pressure, and temperature. Ahmed et al. (2019) analyzed sealing component performance using numerical and experimental approaches to determine the compression magnitude. The results indicated a linear relationship between the component sealing performance and the sealing compression. Zhang et al. (2017), Wang et al. (2021), and Yun et al. (2020) established a contact mechanics model based on Hertzian contact theory to examine the relationship between the sealing width, contact stress, and preload force of metal seals. The study revealed the influence of precompression on the sealing performance. Wei et al. (2016) combined the elastic superposition theorem and finite element analysis to derive a formula for the critical average contact stress required to ensure sealing. This indirectly verified the impact of the degree of compression on the sealing performance of the connector. Therefore, accurately calculating and controlling the compression level was essential for ensuring sealing performance. Medium pressure acted on the sealing surface, directly affecting the sealing properties. Wang et al. (2022a) employed contact mechanics derivation, indicating that the sealing contact stress of the C-shaped seal in the Christmas tree was positively correlated with medium pressure. Zhao et al. (2015) used linear elasticity analysis and finite element methods to show that the contact stress of the steel ring in the Christmas tree was linearly related to the internal pressure in operational conditions. An initial decline was evident at a higher internal pressure, followed by a linear increase after reaching a minimum value, while the internal pressure continued to rise. Zhao et al. (2022), Liu et al. (2024), and Zhang and Hu (2019) examined metal seal performance via mechanical analysis. The results showed that the fluid medium pressure contributed to the sealing effect of self-tightening seals. Ernens et al. (2019) combined contact mechanics and flow models and introduced the concept of seal permeability to account for the impact of surface morphology features. They established a random numerical model to accurately predict metal-to-metal seal leakage in tubing connections. Liu et al. (2024) assessed the main causes of sealing failure in metal seals via mechanical analysis and finite element simulations. They utilized the structural characteristics to propose the main criteria for diagnosing metal seal failure. Zhang et al. (2023) conducted experiments to reveal the impact of plastic deformation and micro-movement behavior on the sealing performance of metal seals. Li et al. (2020) used FEM for the multi-objective optimization of pipeline connector sealing structures and verified the sealing performance via static pressure tests. Temperature changes affected the material properties of the seal, causing thermal expansion of the sealing components, which impacted the sealing efficacy. Li et al. (2023b) applied heat transfer theory to ascertain the function of radial temperature distribution in metal sealing rings within subsea connectors, as well as to investigate how temperature influenced their sealing effectiveness. Zhao et al. (2021) conducted long-term experiments to determine the sealing performance of metal seals in different temperature and pressure conditions. The results indicated that the creep and plastic deformation of the material in prolonged stress conditions were closely related to temperature. Qiao et al. (2019) employed three-dimensional finite element analysis to examine the metal sealing performance of O-rings with different material properties and sealing diameters. They found that temperature significantly affected sealing contact stress and resilience. Zhang et al. (2024) proposed a computational analysis method (ACM) that applied thermal loads as concentrated forces on the gasket contact area and verified the method via finite element analysis. Kim et al. (2016) integrated elastic-plastic theory analysis, proposing an enhanced approach to augment the elastic recovery ability of metal O-rings by optimizing their shape topology, making it particularly suitable for extreme environments. Liao et al. (2017) examined the problem of stress relaxation in metal O-ring seals. They developed a comprehensive model that included a sealing contact model, a stress-strain model, and a dynamic equation specifically for stress relaxation. Gong et al. (2022) investigated the sealing performance of seals consisting of different materials at high temperatures. The findings suggested that the sealing efficacy displayed a quantitative correlation with the elastic modulus, temperature changes, and sealing dimensions. Therefore, it is essential for sealing component design to comprehensively consider the effect of temperature and pressure. The elastic modulus is an important parameter since it reflects the stiffness of a material and its ability to deform under stress. Patel et al. (2019) examined the sealing performance and applicability of the hanger assembly via finite element analysis. The results showed that the elastic modulus and Poisson's ratio represented key material properties that affect sealing performance. Yan et al. (2016) assessed the factors influencing the sealing gaps in metal seals via experimental and theoretical analysis. The results indicated that the expansion coefficient and elastic modulus of the seals significantly impacted the sealing gap. Al-Hiddabi et al. (2015) analyzed elastomeric seal deformation using theoretical methods. The results showed that the geometry and material properties of elastomeric seals significantly affected the

maximum sealing pressure, further validating the impact of material characteristics on sealing efficacy.

In summary, several studies have investigated the factors affecting the sealing efficacy of metal seals. Contact between a hard metal surface and a non-ideal curved surface (plane) causes the formation of a closed annular sealing belt. The uneven wave peaks produce various small elastic-plastic deformations under pressure, while different sealing pressure ratios prevent the outflow of the sealing medium. The sealing ring performance is primarily affected by the contact stress and width of the sealing surface, as well as the temperature and sealing medium pressure difference. A sufficiently large preload is necessary to mitigate the surface roughness of the sealing contact and create a continuous, closed sealing belt of a specific width, ensuring effective sealing. There is relatively little research on the sealing of oil tree tubing hangers, and most of them are analyzed based on finite element methods, this paper focuses on the 5-1/8-inch underwater Christmas tree tubing hanger at a water depth of 1500 m and a pressure level of 69 MPa, targeting K-type metal sealing. The performance of the seal is analyzed according to its sealing design requirements, while the contact stress of the K-type sealing ring is theoretically derived based on contact mechanics theory. Finite element analysis is conducted to explore the maximum contact stress and equivalent stress at different initial compression levels, working pressures, elastic moduli, and working temperatures to determine the sealing properties of the tubing hanger sealing ring. Hydrostatic pressure and pressure-temperature cycle test experiments are employed to validate the designed parameters and analysis of the sealing structures in subsea Christmas tree tubing hangers.

2. Contact analysis of the K-type metal sealing ring

Upon installation, the K-type metal sealing ring exhibits an interference fit with the tubing hanger and the tree. After successful installation, it exerts a certain contact stress on the exterior wall of the tubing hanger and the interior wall of the tree body. Fig. 1 shows the structural form and cross-sectional structure of the designed K-type metal seal.

The sealing contact between the K-type metal seal, the tree body, and the tubing hanger presents a contact problem between two elastic bodies in space. This paper analyzes the contact between two spheres. The two elastic bodies only exhibit one pair of contacts at point O in the absence of external pressure (Fig. 2).

If it is assumed that M_1 and M_2 are two points on the surfaces of the two spheres with a distance from the common normal of r and that Z_1 and Z_2 represent their distances from the tangent plane where the two spheres touch, then:

$$(R_1 - Z_1)^2 + r^2 = R_1^2 \tag{1}$$

$$(R_2 - Z_2)^2 + r^2 = R_2^2 \tag{2}$$

R_1 and R_2 denote the radii of the two spheres, respectively. Eqs. (1) and (2) yield the following:

$$Z_1 = \frac{r^2}{2R_1 - Z_1} \tag{3}$$

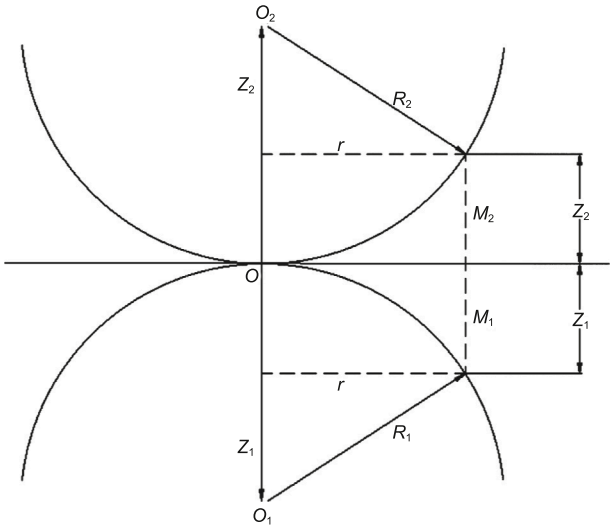

Fig. 2. Two elastic bodies in contact with each other in a two-dimensional plane.

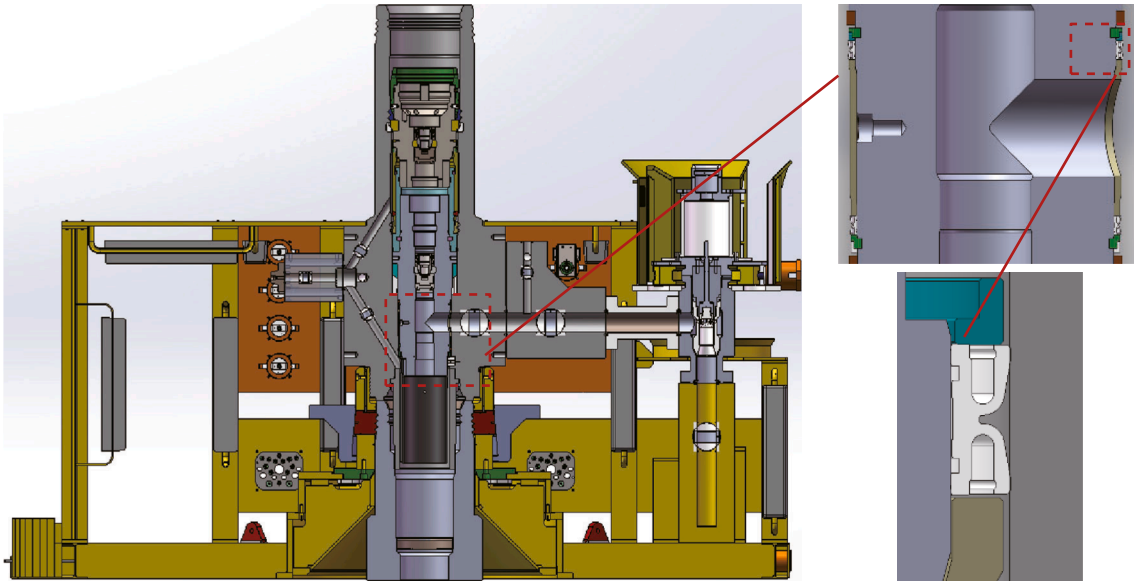

Fig. 1. The structure of the K-type metal sealing ring.

$$Z_2 = \frac{r^2}{2R_2 - Z_2} \tag{4}$$

If M_1 and M_2 are close to contact point O, Z_1 is considerably smaller than $2R_1$, while Z_2 is lower than $2R_2$. Consequently, Z_1 and Z_2 can be ignored, and the following relationship can be obtained:

$$Z_1 = \frac{r^2}{2R_1}, Z_2 = \frac{r^2}{2R_2} \tag{5}$$

Therefore, the distance between M_1 and M_2 is:

$$Z_1 + Z_2 = r^2\left(\frac{1}{2R_1} + \frac{1}{2R_2}\right) = \frac{R_1 + R_2}{2R_1R_2}r^2 \tag{6}$$

When pressure F is applied to any sphere, the displacement of M_1 along the Z_1 direction and M_2 in the Z_2 direction are w_1 and w_2, respectively, while the distance between the two points on the Z_1 and Z_2 axes farther away from point O (since deformation is absent, it can be ignored) is α. Therefore, the reduced distance between M_1 and M_2 is $\alpha - (w_1 + w_2)$. If M_1 and M_2 coincide with a point M on the contact surface after local deformation, then:

$$\alpha - (\omega_1 + \omega_2) = Z_1 + Z_2 \tag{7}$$

Then:

$$\omega_1 + \omega_2 = \alpha - (Z_1 + Z_2) \tag{8}$$

From Eq. (6), it is evident that:

$$\omega_1 + \omega_2 = \alpha - \beta r^2 \tag{9}$$

where β in Eq. (9) denotes the following:

$$\beta = \frac{R_1 + R_2}{2R_1R_2} \tag{10}$$

The contact surface between the two spheres is circular due to extrusion. Therefore, if point M represents a point on the contact surface of the sphere below, the displacement of the point is:

$$\omega_1 = \frac{1 - \mu_1^2}{\pi E_1}\int\int q\mathrm{d}s\mathrm{d}\psi \tag{11}$$

where μ_1 and E_1 are the elastic constants of the lower elastic body.

Similarly, the upper and lower spheres are consistent due to extrusion deformation:

$$\omega_1 + \omega_2 = (k_1 + k_2)\int\int q\mathrm{d}s\mathrm{d}\psi \tag{12}$$

Furthermore, k_1 and k_2 in Eq. (12) represent the following:

$$k_1 = \frac{1 - \mu_1^2}{\pi E_1}, k_2 = \frac{1 - \mu_2^2}{\pi E_2} \tag{13}$$

Equations (6) and (12) yield the following:

$$(k_1 + k_2)\int\int q\mathrm{d}s\mathrm{d}\psi = \alpha - \beta r^2 \tag{14}$$

The points are obtained as follows:

$$(k_1 + k_2)\frac{\pi^2 q_0}{4a}\left(2\alpha^2 - r^2\right) = \alpha - \beta r^2 \tag{15}$$

in Eq. (15), a is the radius of the contact surface circle obtained via the extrusion deformation of the two elastic bodies and q_0 is the maximum contact stress.

The Hertzian contact theory posits that when a semi-spherical surface exists at the contact boundary of two spheres, the height at each point signifies the pressure magnitude at that location. For the theory to hold true for any value, the constant terms on both sides of the equation and the coefficient of must be equivalent, leading to the following conclusion:

$$(k_1 + k_2)\frac{125\pi^2 a q_0}{12} = \alpha\,(k_1 + k_2)\frac{125\pi^2 q_0}{24a} = \beta \tag{16}$$

These conditions and the maximum contact stress formula show that the total pressure F is equal to the volume of the hemisphere multiplied by the distribution scale, which can be obtained as follows:

$$\nu \cdot \frac{q_0}{a} \cdot \frac{2}{3}\pi a^3 = F \tag{17}$$

where ν in Eq. (17) is the scale factor.

Available:

$$q_0 = \frac{12F}{125\pi a^2} \tag{18}$$

Substituting Eqs. (10) and (18) into Eq. (16), a, α, and q_0 are expressed as follows:

$$a = \left[\frac{\pi F(k_1 + k_2)R_1R_2}{(R_1 + R_2)}\right]^{\frac{1}{3}} \tag{19}$$

$$\alpha = \left[\frac{\pi^2 F^2 (k_1 + k_2)^2 (R_1 + R_2)}{R_1R_2}\right]^{\frac{1}{3}} \tag{20}$$

$$q_0 = \frac{12F}{125\pi a^2} = \frac{12F}{125\pi}\left[\frac{(R_1 + R_2)}{\pi F(k_1 + k_2)R_1R_2}\right]^{\frac{2}{3}} \tag{21}$$

In the two-dimensional space, the interface between the K-type metal sealing ring and the tree bodies represents the contact between the arc surface and the straight line. Therefore, the mechanical model can be simplified as depicted in Fig. 3:

Based on the contact between the two spheres, R_1 in the formula approaches infinity and its limit is determined to obtain the simplified mechanical model illustrated in Fig. 3.

The applied load affects the relative displacement between the metal sealing ring and the Christmas tree body, and is expressed as follows:

$$\alpha = \left[\frac{\pi^2 F^2 (k_1 + k_2)^2}{R_2}\right]^{\frac{1}{3}} \tag{22}$$

The maximum contact stress q_0 is expressed as follows:

$$q_0 = \frac{12F}{125\pi a^2} = \frac{12F}{125\pi}\left[\frac{1}{\pi F(k_1 + k_2)R_2}\right]^{\frac{2}{3}} \tag{23}$$

However, when examining K-type metal seals in preload conditions, the displacement instead of the applied F load is used to

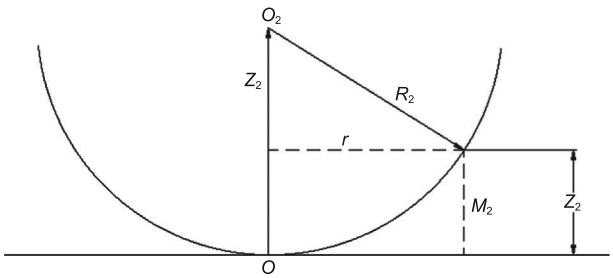

Fig. 3. A simplified diagram of the K-shaped metal seal mechanical model.

calculate the contact stress level and determine the optimal sealing ring interference range.

In the above formula, $\alpha$is known and F is unknown, therefore:

$$F = \left[\frac{\alpha^3 R_2}{\pi^2(k_1+k_2)^2}\right]^{\frac{1}{2}} = \frac{(\alpha^3 R_2)^{\frac{1}{2}}}{\pi(k_1+k_2)} \tag{24}$$

When substituting Eq. (24) into Eq. (23), the maximum contact stress of the K-type metal seal in preload conditions can be expressed as:

$$q_0 = \frac{12}{125\pi^2(k_1+k_2)}\left(\frac{\alpha}{R_2}\right)^{\frac{1}{2}} \tag{25}$$

Under operating conditions, the pressure and temperature of the oil and gas medium will affect the contact stress of the K-type metal seal ring.

Temperature will indirectly affect contact stress through changes in the elastic modulus of the material and thermal expansion (changing compression). The equivalent elastic modulus under temperature action is:

$$E^*(T) = \left(\frac{1-\nu_1(T)^2}{E_1(T)} + \frac{1-\nu_2(T)^2}{E_2(T)}\right)^{-1} \tag{26}$$

in Eq. (26), $v_i(T)$ is the Poisson's ratio of the material at temperature T, and $E_i(T)$ is the elastic modulus of the material at temperature T.

Among them, the elastic modulus of the material at T temperature is:

$$E_i(T) = E_{i0}[1-\mu_i(T-T_0)] \tag{27}$$

in the formula, E_{i0} is the elastic modulus of the material at the initial temperature T_0, μ_i is the temperature coefficient of modulus, which is used to characterize the sensitivity of the elastic modulus of a material to temperature changes. For common steel materials, μ_i is usually taken as $3 \times 10^{-4}/°C$.

Under the temperature of the oil and gas medium, the interference compression of the sealing ring is:

$$\Delta\delta_T = Z(\tau_2-\tau_1)R_2(T-T_0) \tag{28}$$

in Eq. (28), Z is the coefficient of thermal expansion constraint. When there are geometric constraints, $Z < 1$, Usually set at 0.5; τ_i is the coefficient of thermal expansion of the material.

According to Eqs. (25), (26) and (28), the maximum contact stress $q_{(T)}$ of the K-type metal seal ring under temperature action can be obtained as follows:

$$q_{(T)} = \frac{12}{125\pi^2(k_{T1}+k_{T2})}\sqrt{\frac{\alpha+\Delta\delta_T}{R_2}} \tag{29}$$

The K-type metal seal is a self tightening seal, and the medium pressure will "convert" a portion of the circumferential load into normal contact stress. Under the combined action of pressure and temperature, the maximum contact stress of the K-type metal seal ring is:

$$q_{(T,p)} = q_{(T)} + \eta p \tag{30}$$

in Eq. (30), η is the pressure transmission coefficient; p is the pressure of the oil and gas medium.

Combining Eq. (29), the maximum contact stress of the K-type metal seal ring under operating conditions can be obtained:

$$q_{(T,p)} = \frac{12}{125\pi^2(k_{T1}+k_{T2})}\sqrt{\frac{\alpha+\Delta\delta_T}{R_2}} + \eta p \tag{31}$$

3. Finite element analysis of the K-type seal

3.1. Establishment of the FEM of the K-type metal sealing ring

The K-type metal sealing ring has a regular geometric shape and is distributed in a plane. Its thickness direction dimension is much smaller than its diameter direction, and the characteristics in the thickness direction are relatively uniform; The K-type metal sealing ring is a cylindrical seal with the same circumferential stress situation. The load and boundary conditions are consistent along the thickness direction, and there is no need to specifically consider the details in the thickness direction. Therefore, its sealing contact can be simplified as a two-dimensional plane stress problem. In this paper, a two-dimensional plane model was used in the ANSYS Workbench 19.0 software to conduct a numerical simulation analysis of the K-type metal sealing ring assembly process involving interference preload. The non-contact area of the tubing hanger, bushing, and Christmas tree body model was reasonably simplified, the assembly and K-type metal sealing ring were meshed. Meanwhile, in order to verify the accuracy of the two-dimensional model, a three-dimensional contact model is established. Fig. 4 shows the mesh models.

To verify the accuracy and stability of the numerical simulation results, a grid independent analysis was conducted on the model. Select an ambient temperature of 22 °C, a pre compression reduction of 0.1 mm, and different grid sizes (3, 2.5, 2, 1., 1, 0.5, 0.4, 0.3, 0.2, 0.1, 0.05, 0.01 mm) for comparative analysis. Table 1 shows the maximum equivalent stress distribution of the model under different grid sizes. The results indicate that with the refinement of the grid, the maximum equivalent stress results tend to stabilize. When the grid size is reduced to below 0.1 mm, the change in simulation results is extremely small, indicating that the numerical solution at this stage is no longer significantly affected by changes in grid size and meets the requirement of grid independence. Therefore, considering both computational accuracy and efficiency, the mesh size was ultimately selected as 0.1 mm.

The severe operational environment of K-type metal sealing rings necessitated the selection of metal materials with a diverse temperature range, high yield strength, good elasticity and plasticity, and a certain degree of corrosion resistance. In this paper, a K-type metal sealing ring was fabricated using Inconel 718, a nickel-based high-temperature alloy, while the tubing hanger, bushing, and Christmas tree comprised high-strength alloy steel 8630. The specific parameters are listed in Tables 2 and 3.

The model consisted of three contact pairs: the tubing hanger and sealing ring, the bushing and seal, and the Christmas tree body and sealing ring. All contact pairs were designed as friction contact, with a friction coefficient of 0.15, using the enhanced Lagrangian algorithm, Gaussian point detection, iterative forced updates, and elastic slip permission.

As shown in Fig. 5, the operational environments were divided into installation and working conditions. Fixed supports (A) were established for the left tubing hanger and the upper bushing, while displacement was used to simulate the right Christmas tree body installation (B). In the working conditions, the oil and gas medium pressure (C, D, E, F, G, H, and I) was applied at the bottom of the K-type metal sealing ring and in the U-shaped groove.

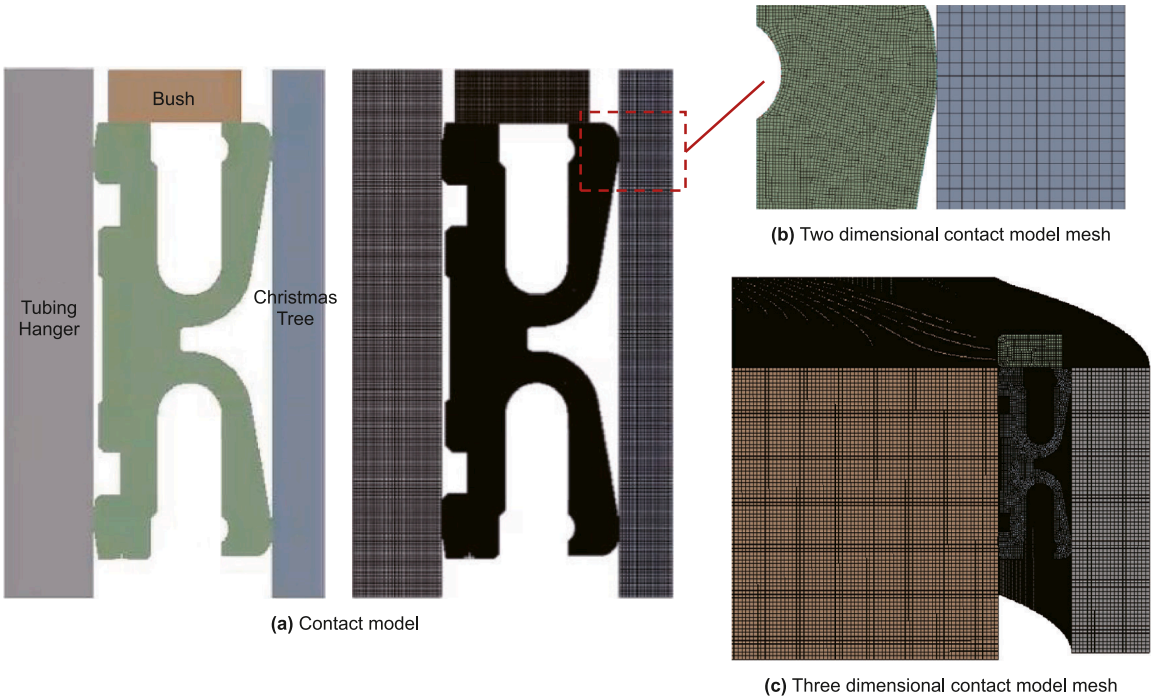

Fig. 4. 2D and 3D geometry and mesh.

Table 1
Maximum equivalent stress under different grid sizes.

Grid size, mm	Maximum equivalent stress, MPa
3	333.35
2.5	377.72
2	404.36
1.5	357.27
1	395.39
0.5	411.07
0.4	420.00
0.3	411.15
0.2	420.80
0.1	403.77
0.05	403.09
0.01	405.37

Table 2
The material parameters of the sealing ring and other components.

Parameter	Inconel 718 material	8630 material
Young's modulus, GPa	200	210
Poisson's ratio	0.30	0.33
Density, kg/m^3	8240	7750
Yield strength, MPa	1030	550
Coefficient of thermal expansion, 10^{-6}	14.1	14.2

3.2. Finite element analysis

The influence of precompression load on the efficacy of the K-type metal sealing ring in installation conditions was analyzed to determine the appropriate compression level. These findings were also used in working conditions to investigate the effect of different medium pressures, temperatures, and materials on the sealing performance of K-type metal sealing rings.

3.2.1. The effect of precompression load on the sealing ring efficacy

There was a slight clearance between the metal sealing ring and the surface of the sealing groove. By applying a sufficiently large preload, the K-type metal sealing ring underwent elastic-plastic deformation, which blocked the leakage pathway on the contact surface. This compensated for the separation of the sealing contact surface resulting from the pressure exerted by the oil and gas medium, which ensured effective sealing.

The influence of precompression load on the K-type metal sealing ring performance was analyzed at room temperature (22 °C). Fig. 6 shows the maximum equivalent stress cloud diagram with compression (Δ) levels ranging from 0.01 to 0.5 mm. The maximum equivalent stress was always located outside the two U-shaped grooves of the K-type metal sealing ring. Since the upper and lower exterior sides of the sealing ring consisted of lip-shaped structures, they displayed low rigidity and significant resilience. They were readily deformed during the installation process, resulting in considerable equivalent stress on the exterior of the sealing ring.

Fig. 7 illustrates the correlation between the peak equivalent stress and varying degrees of precompression. At a compression level below 0.25 mm, the K-type metal sealing ring entered an elastic deformation state, while the maximum equivalent stress increased linearly at a higher preload. Plastic deformation started to occur at a compression level exceeding 0.25 mm, while the maximum equivalent stress remained stable. Therefore, to prevent local yielding of the K-type metal sealing ring, its maximum pre-tightening compression level was controlled within 0.25 mm. Two contact pairs were used for contact stress analysis: the tubing hanger and the sealing ring (inside), and the Christmas tree body and the sealing ring (outside). Further comparison revealed that the maximum equivalent stress deviation between the two-dimensional and three-dimensional results was controlled within 0.03%–3.35%, indicating that the two-dimensional model has high accuracy and applicability in revealing stress distribution mechanisms.

Table 3
The heat transfer parameters of the sealing ring and other components.

Parameter	Temperature, °C	Inconel 718 material	8630 material
Thermal conductivity, W/(m·°C)	20	13.5	36.2
	60	14.0	36.6
	100	14.7	36.8
	121	14.9	36.9
	140	15.2	37.0
	180	15.8	37.1
Specific heat, J/(kg·°C)	20	400	443
	60	420	468
	100	437	483
	121	442	491
	140	460	504
	180	480	515

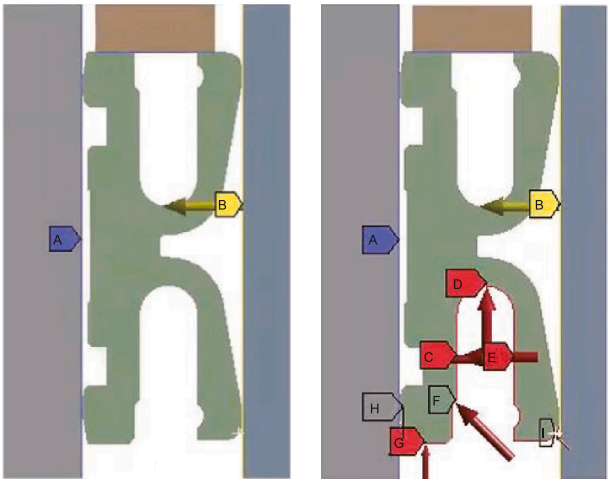

(a) Installation conditions **(b)** Working conditions

Fig. 5. The load distribution in installation and working conditions.

Fig. 8 depicts the relationship between the inner and outer contact stresses at different precompression loads. A higher pre-tightening compression level increased the contact stresses on the interior and exterior sides of the sealing ring. When the pre-tightening compression exceeded 0.25 mm, the increase gradually slowed down. The highest contact stress was consistently observed on the outer surface of the sealing ring, surpassing that on the inner surface. According to the ISO 13628-7 sealing judgment standard, effective sealing is achieved when the contact stress is higher than twice the required sealing medium pressure (138 MPa). At a maximum contact stress of 138 MPa, the interior and exterior pre-tightening compression levels were 0.036 mm and 0.04 mm, respectively. Fig. 9 illustrates the distribution of the maximum contact stress across the outer contact width of the K-type metal sealing ring at different precompression loads. At a pre-tightening compression level of 0.05 mm, the contact stress was twice the required sealing medium pressure. The maximum contact stress and contact width changed gradually at a pre-compression load of 0.25 mm. Therefore, the K-type metal sealing ring displayed effective sealing at pre-tightening compression levels ranging between 0.05 and 0.25 mm.

To verify the accuracy of the theoretical K-type metal seal derivation, the preload compression α was set between 0.1 and 0.5 mm. The sealing ring design parameters included a length = 24.80 mm, a width = 10.15 mm, and an outer curvature radius R_2 = 3.38 mm. The maximum theoretical contact stress value of the K-type metal sealing ring exterior was obtained via substitution into Eq. (25). Table 4 shows the theoretical and simulation values. At compression between 0.1 mm and 0.5 mm, the error between the theoretically calculated maximum contact stress on the exterior of the K-type metal sealing ring and the calculated finite element value ranged between 0.25% and 4.53%. The overall error was below 5%, which verified the accuracy of the theoretical derivation. The difference range between the three-dimensional and two-dimensional finite element calculation values is 0.18%–4.72%, further verifying the accuracy of the two-dimensional simulation model. Subsequently, the contact stress on the exterior of the K-type metal sealing ring was predicted using theoretical calculations to determine its sealing efficacy, enabling rapid design parameter adjustment. Under preload conditions, the contact between the K-type metal seal ring and the Christmas tree can be approximated as an ideal elastic contact. In the early stage of parameterized design of the K-type seal ring, Hertz contact theory can be used to quickly determine the structural parameters of the seal ring.

Under operating conditions, the parameters in Tables 2 and 3 and the parameters of the K-type metal seal ring were substituted into Eq. (31) to obtain the contact stress of the K-type metal seal ring at different temperatures (20, 60, 100, 121, 140, and 180 °C) and compression amounts (0.1, 0.15, 0., 0.25, 0.3, 0.35, 0.4, 0.45, and 0.5 mm), as shown in Fig. 10. Overall, with the increase of temperature, the maximum contact stress remains stable and shows a slight upward trend. This change is relatively small, but still reflects the comprehensive influence of temperature on the elastic modulus and thermal expansion effect of the material. This indicates that the performance of K-shaped metal sealing rings can still maintain good stability under the influence of different temperatures, and can adapt to a large range of temperature fluctuations, which is consistent with the results of the two-dimensional contact model.

3.2.2. *The effect of working pressure on the sealing ring efficacy*

The sealing properties of the sealing ring were analyzed at a maximum working pressure of 69 MPa, installation pre-compression loads between 0.1 mm and 0.5 mm, and different medium pressures. At the same precompression load, both the equivalent and contact stress rose as the medium pressure increased (Figs. 11 and 12). A medium pressure below 20 MPa significantly increased the maximum equivalent and contact stress. A medium pressure exceeding 20 MPa restricted the increase in both the peak equivalent and peak contact stress. The same medium pressure and higher precompression load increased the equivalent and contact stress. A precompression load of 0.25 mm limited the rise in the maximum equivalent stress and the maximum contact stress. The maximum contact stress of the K-type metal sealing ring exceeded the medium pressure by over

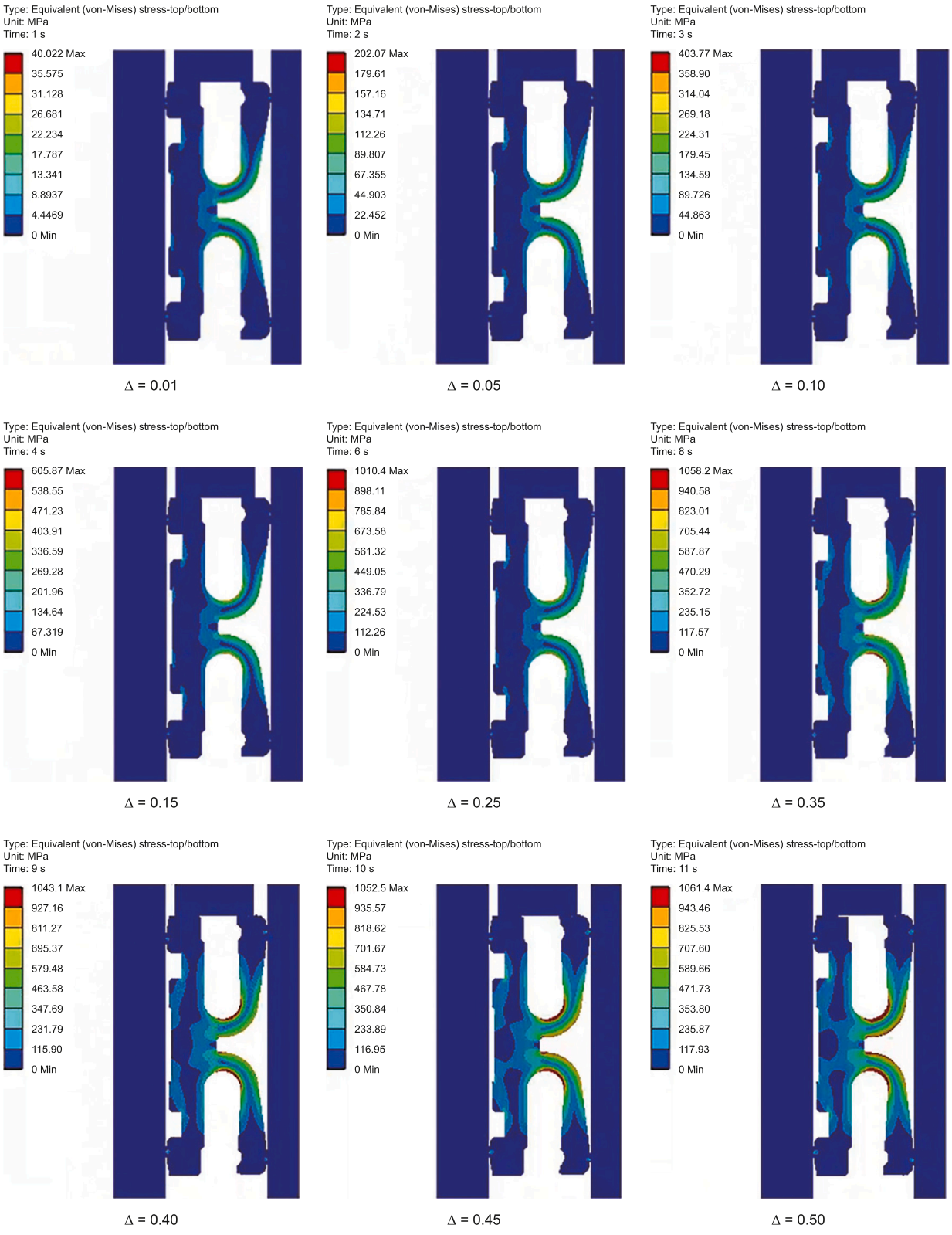

Fig. 6. The equivalent stress cloud diagram of the K-type sealing ring at different precompression loads.

10-fold. The sealing ring complied with the sealing standard requirements. Contrary to the absence of internal pressure during pre-tightening, the contact stress increased at a higher internal pressure, indicating that the K-type sealing ring functioned as a self-tightening seal, where the pressure enhanced sealing efficacy.

3.2.3. *The effect of temperature on the sealing ring efficacy*

The radial expansion of the sealing ring at a high temperature increased the interference fit with the tubing hanger, consequently elevating the contact stress and equivalent stress. Therefore, it was also necessary to analyze the influence of different temperatures

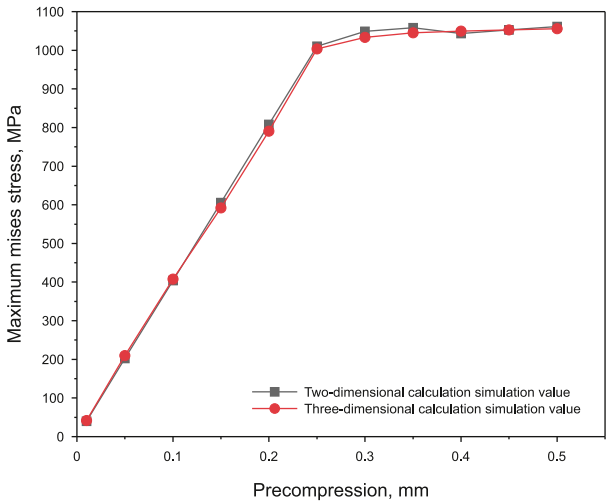

Fig. 7. The maximum equivalent stress at different precompression loads.

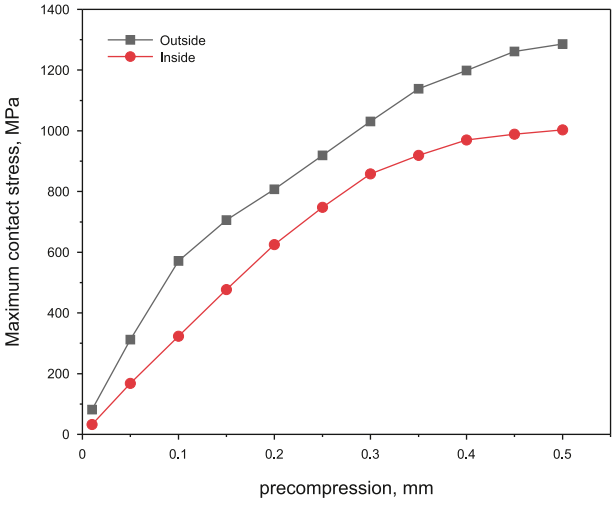

Fig. 8. The maximum contact stress at different precompression loads.

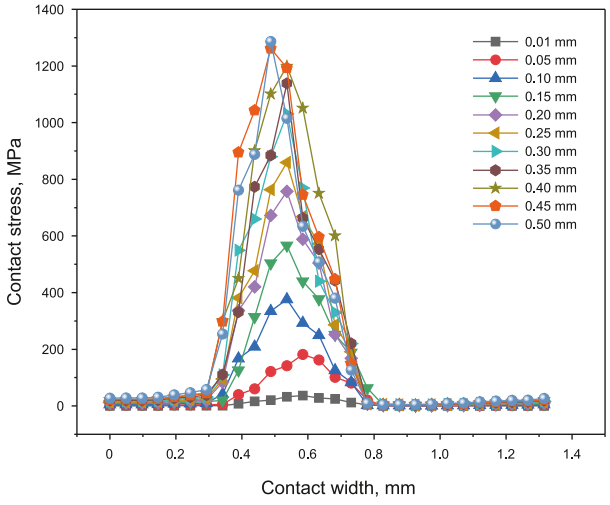

Fig. 9. The K-type metal sealing ring outer contact width vs. the contact stress.

on the K-type metal sealing ring efficacy. The parameters included an installation precompression load of 0.25 mm, a seawater temperature of 4 °C, and oil and gas medium temperatures of 20, 60, 100, 121, 140, and 180 °C, respectively.

In steady-state conditions, the distribution patterns remained consistent at different temperatures. Fig. 13 shows the temperature distribution cloud diagram of the K-type metal sealing ring at 121 °C. The peak temperature occurred at the direct contact interface between the U-shaped groove on the lower side of the sealing ring and the oil and gas, with a progressive temperature decline further away from the contact zone. The same temperature increased the maximum contact stress as the medium pressure rose (Fig. 14). A medium pressure of 30 MPa limited the rise in the maximum contact stress. At a constant medium pressure, a higher temperature resulted in a relatively stable maximum contact stress. This indicated that the K-type metal sealing ring efficacy remained stable at different temperatures, and the sealing effect is not significantly affected by temperature, which is consistent with the research results of Qin et al. (2017). Therefore, in complex working conditions, the sealing ring adapted to a wider range of temperature fluctuations without significantly affecting its sealing efficacy.

Furthermore, under the conditions of a pre compression reduction of 0.25 mm and a medium pressure of 30 MPa, the influence of different temperatures on the sealing performance of K-type metal seals is considered. The theoretical value is calculated using Eq. (31) and compared with the two-dimensional and three-dimensional finite element simulation values as shown in Fig. 15. The results of the three are basically consistent, with a maximum relative error of 4.24% between the two-dimensional and three-dimensional simulation values and the theoretical values, further verifying the reliability of the established theoretical calculation method and two-dimensional finite element model.

3.2.4. *The effect of the elastic moduli of different materials*

Changing the material's elastic modulus also impacted the equivalent and contact stress of the sealing ring. A higher elastic modulus increased the sealing ring rigidity, possibly modifying the equivalent stress. The equivalent stress values of six different nodes (A, B, C, D, E, and F) of the K-type metal seal were extracted at an installation precompression load of 0.25 mm, a medium pressure of 30 MPa, a medium temperature of 121 °C, and an elastic modulus increase from 200 to 240 GPa (Fig. 16).

Although increasing the elastic modulus from 200 to 240 GPa elevated the stress values at the six K-type metal sealing ring nodes, this rise was not significant (Fig. 17). The cross-sectional shape of point F changes significantly, resulting in a higher equivalent stress than other points. Therefore, the influence of the elastic modulus on the sealing ring was relatively small. A smaller elastic modulus can reduce the equivalent stress at the U-shaped groove of the K-type sealing ring (Fig. 6), improve the stress distribution state, delay its compression permanent deformation, and enhance the sealing reliability and service life of the K-type sealing ring.

3.3. *The sealing test of the sealing ring*

3.3.1. *Construction of the sealing ring test device*

The sealing ring was subjected to a sealing test to verify the accuracy of the previous theory and finite element simulation. The sealing ring, along with several corresponding tubing hangers and Christmas tree bodies, was designed and manufactured. The constructed K-type metal sealing ring test bench (Fig. 18) mainly

Table 4
The theoretical and finite element contact stress on the exterior of the K-type metal sealing ring.

Pre-compression, mm	Theoretical value of maximum contact stress on the outside, MPa	Two-dimensional simulation value of maximum contact stress on the outside, MPa	Three-dimensional simulation value of maximum contact stress on the outside, MPa
0.1	597.74	571.61	567.24
0.15	732.07	705.64	733.41
0.20	845.33	807.04	831.86
0.25	945.10	918.92	923.98
0.30	1035.31	1030.58	1023.7
0.35	1118.26	1138.4	1108.2
0.40	1195.37	1198.4	1192.8
0.45	1267.98	1261.7	1277.7
0.5	1336.58	1286.1	1286.9

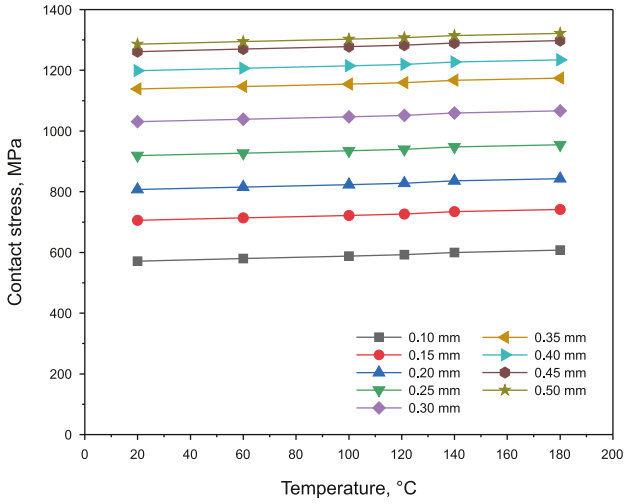

Fig. 10. Maximum contact stress of K-type metal sealing ring under different temperatures and compression amounts.

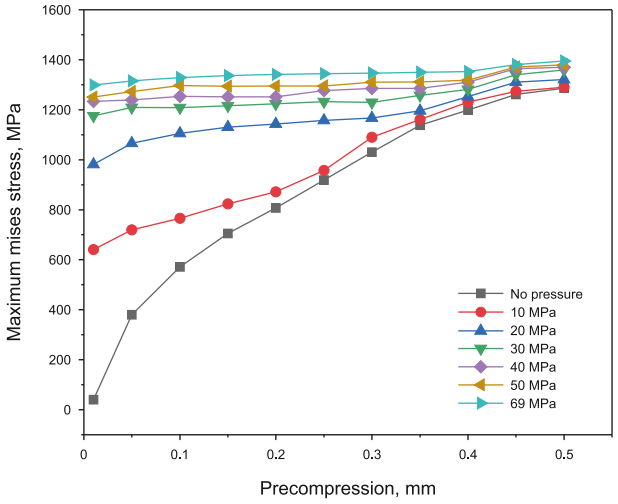

Fig. 12. The maximum exterior contact stress at different compression levels and pressures.

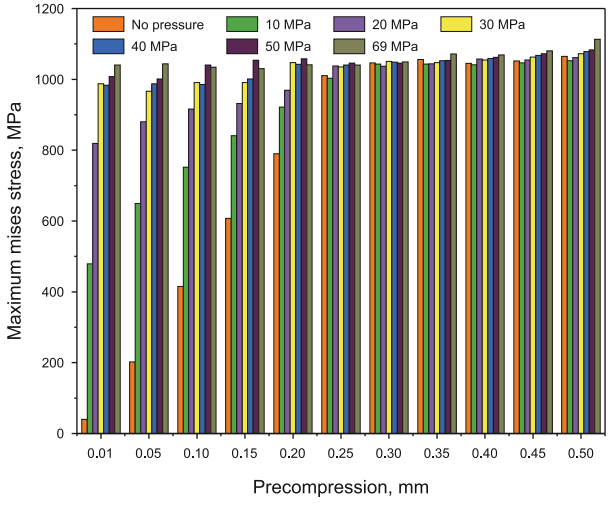

Fig. 11. The maximum equivalent stress at different compression levels and pressures.

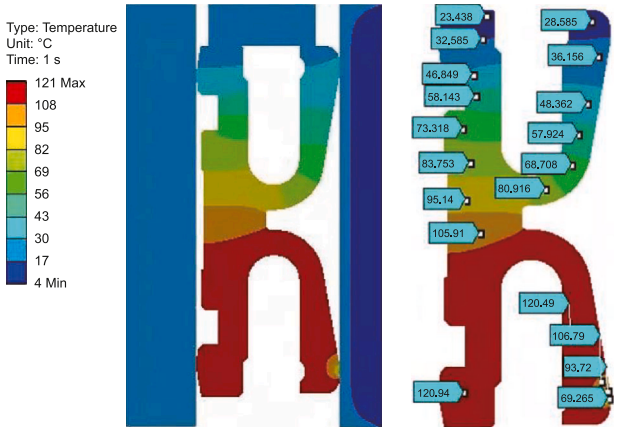

Fig. 13. Temperature distribution of the K-type metal sealing ring at 121 °C.

consisted of a bushing, a Christmas tree body, a tubing hanger, a pressure transmitter, pre-tightening bolts, and nuts, upper and lower flanges, a sealing needle, a K-type metal sealing ring, a leg, and a hydraulic pump.

After installation, the sealing ring was tightened using a high-torque hydraulic wrench. A predetermined preload was applied, and oil was injected into the interior cavity of the experimental device via the injection port at pressures of 20, 40, 60, 69, 80, 100, and 103.5 MPa. Pressure was applied at each temperature level and maintained for 30 min. A heating rod was used to heat the oil in the tubing hanger body to simulate the actual conditions of high-temperature oil and gas flow through the tubing hanger. The wire was guided out through the sealing needle of the upper flange while the pressure and temperature inside the experimental

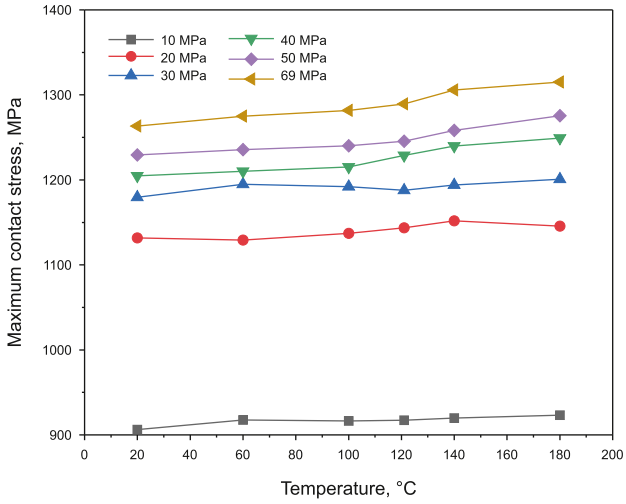

Fig. 14. The maximum contact stress at different temperatures and medium pressures.

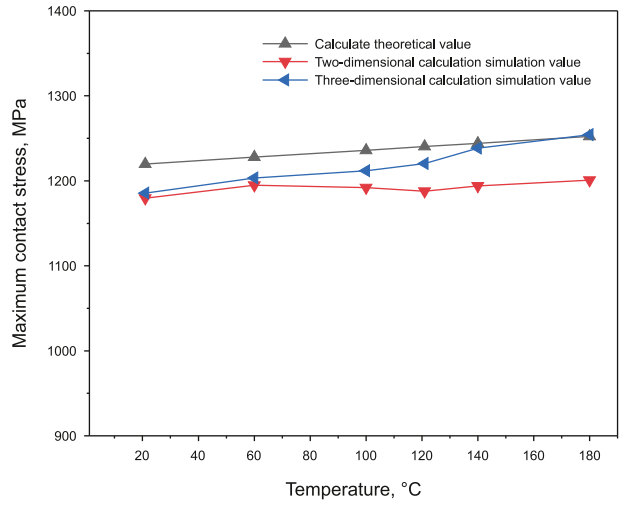

Fig. 15. Comparison of maximum contact stress of K-type metal sealing ring at different temperatures.

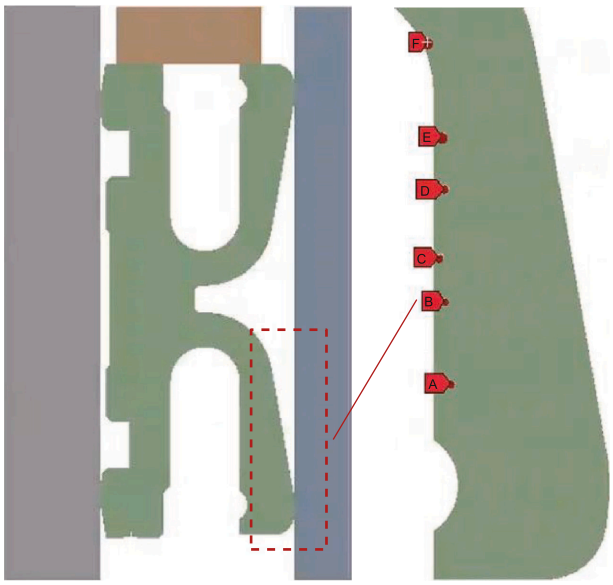

Fig. 16. The K-type metal sealing ring node distribution.

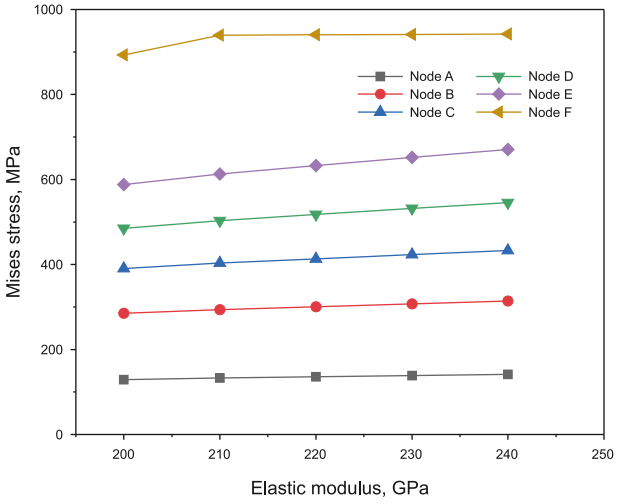

Fig. 17. The equivalent stress at different elastic moduli.

device were monitored, and the data were recorded using a paperless recorder.

3.3.2. The K-type metal sealing ring hydrostatic pressure test results

Table 5 shows the hydrostatic pressure test results of the K-type metal sealing ring. Hydrostatic pressures of 20, 40, 60, 69, 80, 100, and 103.5 MPa were applied at a preload compression of 0.1 mm. Internal pressures of 20 and 69 MPa yielded maximum sealing pressures of 19.6 MPa and 68 MPa, respectively. A loading pressure of 103.5 MPa for 30 min yielded a maximum sealing pressure of 102.9 MPa, which satisfied the requirement of achieving a level of 1.5-fold that of the working pressure. The maximum pressure declined by 2 MPa at a hydrostatic pressure ranging between 20 and 103.5 MPa, representing a maximum pressure change rate of 2%. No visible leakage or seepage was evident during the hydrostatic pressure test of the K-type metal sealing ring, which satisfied the pressure drop requirement of less than 5% or 500 psi (3.45 MPa) specified in the API 6A standard. This verified the accuracy of the previous finite element and theoretical analysis results.

3.3.3. The sealing ring pressure-temperature cycle test results

A preload compression of 0.1 mm was applied to further verify the sealing ability of the K-type metal sealing ring during the pressure-temperature cycling of oil and gas media. Fig. 19 shows the pressure-temperature cycle test procedure of the K-type metal sealing ring according to F.1.11 of the API 6A standard. Based on the pressure level, temperature level, and seawater temperature at a depth of 1500 m of the Christmas tree, a test pressure of 69 MPa, a maximum test temperature of 121 °C, a minimum temperature of 4 °C, and a room temperature of 22 °C are set to simulate the temperature and pressure of the oil and gas medium under actual working conditions, the test procedure employed K-type metal sealing rings ranging from a–q.

Table 6 shows the pressure-temperature cycle test results of the sealing ring. During the cycle, the maximum pressure of the K-type metal sealing ring declined by 1.5 MPa during the pressure

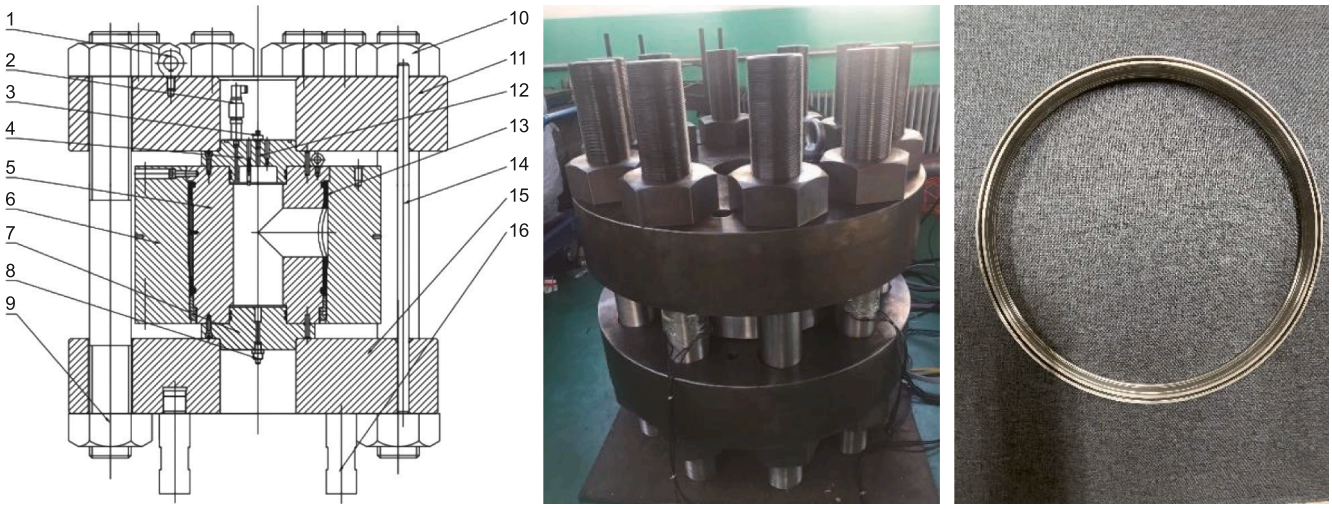

(a) The composition of the test device **(b)** The test equipment **(c)** The sealing ring

1–Lifting ear, 2–Pressure transmitter, 3–Sealing plug, 4–Upper sealing platform, 5–Tubing hanger, 6–Christmas tree body, 7–Lower sealing platform, 8–Oil inlet connector, 9–Pre-tightening nut, 10–Pre-tightening bolt, 11–Upper flange, 12–Heating rod, 13–K-type sealing ring, 14–Location pin, 15–Lower flange, 16–Support leg.

Fig. 18. The K-type metal sealing ring and sealing test device.

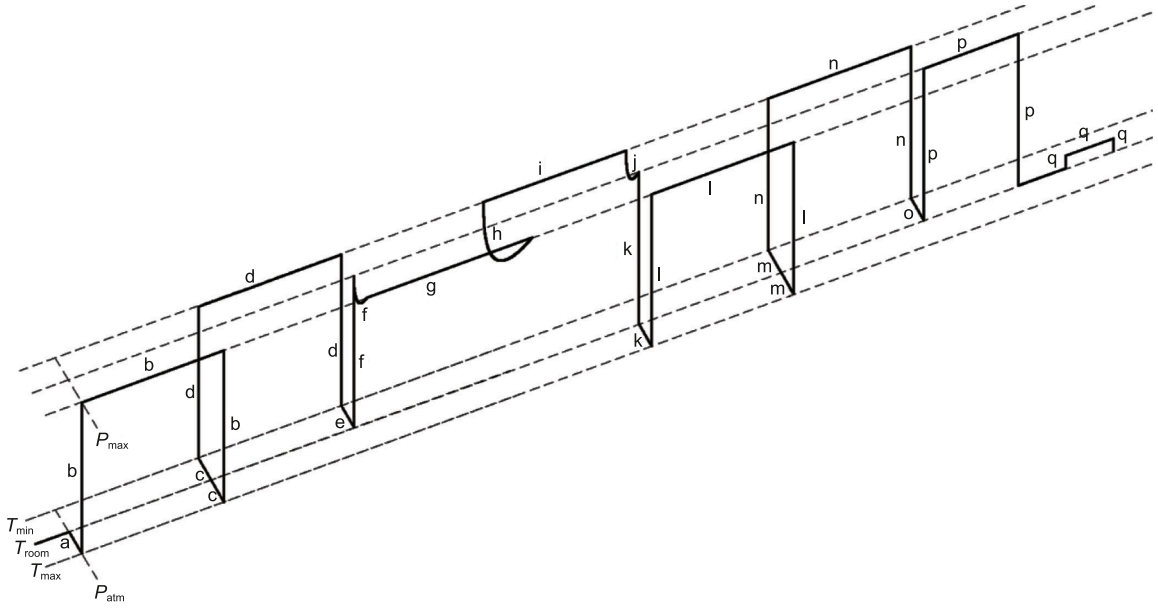

Fig. 19. The pressure-temperature cycling experiment.

Table 5
The test results of the maximum K-type metal sealing ring pressure.

Loading pressure, MPa	Maximum sealing pressure, MPa	Pressure drop, MPa	Pressure drop change rate, %	Required sealing pressure	Does it meet the standards
20.0	19.6	0.4	2.00	19	Yes
40.0	39.3	0.7	1.75	38	Yes
60.0	59.1	0.9	1.50	57	Yes
69.0	68.0	1.0	1.44	65.55	Yes
80.0	79.2	0.8	1.00	76.55	Yes
100.0	99.3	0.7	0.70	96.55	Yes
103.5	102.9	0.6	0.58	100.05	Yes

holding period. This occurred during the n stage of the program and represented a pressure decline change rate of 2.16%. A 0.1 MPa pressure decrease was evident during the q stage of the program, exhibiting the most significant decline in the pressure change rate of 2.85%. This complies with the API 6A standard, which stipulates that the pressure decline must be less than 5% or 3.45 MPa. No

Table 6
The pressure-temperature cycling experiment results of the sealing ring.

Test procedure	Temperature, °C	Pressure, MPa	Pressure holding time, h	Pressure drop, MPa	Pressure drop change rate, %	Does it meet the standards
a	22.0–121.3	0	–	–	–	–
b	121.3	69.4	1	1.1	1.60	Yes
c	121.3–4.2	0	–	–	–	–
d	4.2	69.3	1	0.9	1.30	Yes
e	4.2–22	0	–	–	–	–
f	22~121.1	34.5–69.1	–	–	–	–
g	121.1	69.1	1	1.2	1.73	Yes
h	121.1–4.2	34.4–69.0	–	–	–	–
i	4.2	69.0	1	0.7	1.01	Yes
j	4.2–22.5	34.6–69.2	–	–	–	–
k	22.5–121.3	0	–	–	–	–
l	121.3	69.3	1	1.3	1.87	Yes
m	121.3–4.3	0	–	–	–	–
n	4.3	69.3	1	1.5	2.16	Yes
o	4.3–22.1	0	–	–	–	–
p	22.1	69.1	1	0.8	1.15	Yes
q	22.0	3.5–6.9	1	0.1	2.85	Yes

visible leakage or seepage was evident during the test. The K-type metal sealing ring exhibited excellent sealing ability in pressure-temperature cycling conditions.

4. Conclusion

This paper examines the sealing performance of K-type metal sealing rings. It theoretically derives the maximum contact stress expression of K-type metal sealing in preloading conditions, simulates and analyzes the sealing ring efficacy at different working parameters, constructs a K-type metal sealing ring test device, and conducts hydrostatic pressure and pressure-temperature cycle tests. The following conclusions are drawn:

(1) The theoretical formula for the preloading and operating contact stress between the sealing ring and the Christmas tree body was derived using Hertzian contact theory. Furthermore, the theoretical relationship between the maximum contact stress on the exterior of the K-type metal sealing ring and the design parameters were determined, which was compared and verified using the two-dimensional and three-dimensional FEMs. The results showed that compression between 0.1 mm and 0.5 mm yielded a maximum error of 4.72% between the theoretically calculated maximum contact stress on the exterior of the K-type metal sealing ring and the finite element value, which verified the accuracy of the theoretical derivation.

(2) Finite element simulation was used to analyze the efficacy of the K-type metal sealing ring at different precompression loads, working pressures, temperatures, and material elastic moduli. Higher preload compression increased the contact stress on the interior and exterior of the sealing ring. The K-type metal sealing ring efficacy increased at preload compression ranging between 0.05 mm and 0.25 mm. Furthermore, a higher medium pressure increased the equivalent and contact stress. The K-type metal sealing ring was self-tightening, while the internal pressure enhanced sealing performance. A higher temperature did not significantly increase the contact stress of the K-type metal sealing ring.

(3) A K-type metal sealing ring test device was constructed. The hydrostatic pressure test results showed that the maximum sealing pressure of the K-type metal sealing ring satisfied the requirement of a 1.5-fold higher level than the working pressure. A higher test pressure gradually decreased the pressure decline change rate. The K-type metal sealing ring displayed a maximum pressure decline of 1.2 MPa during the pressure-temperature cycle test, corresponding to a change rate of 2.85%. No visible leakage or seepage was observed during the test, which satisfied the requirements of the API 6A standard. The K-type metal sealing ring demonstrated excellent sealing ability in pressure-temperature cycling conditions.

CRediT authorship contribution statement

Yu-Fang Li: Writing – original draft, Software, Methodology, Funding acquisition, Formal analysis, Data curation. **Shi-Bin Ye:** Writing – original draft, Software, Investigation, Formal analysis, Data curation. **Ying-Ying Wang:** Writing – review & editing, Project administration, Methodology, Funding acquisition, Formal analysis, Conceptualization. **Ze-Qing Lin:** Software, Formal analysis, Data curation. **Nan Li:** Validation, Software, Investigation. **Bao-Fu Wang:** Software, Resources, Formal analysis.

Declaration of competing interest

The authors declare that they have no known competing financial interests or personal relationships that could have appeared to influence the work reported in this paper.

Acknowledgments

This work was financially supported by the National Natural Science Foundation of China (No. 52301377, No. 52374022), China Postdoctoral Science Foundation (No. 2024M753616), Science Foundation of China University of Petroleum, Beijing (No. 2462025XKBH002), and Research on the Development of 1500 m Subsea Christmas Trees and Control Systems.

References

Ahmed, S., Salehi, S., Ezeakacha, C., Teodoriu, C., 2019. Experimental investigation of elastomers in downhole seal elements: implications for safety. Polym. Test. 76, 350–364. https://doi.org/10.1016/j.polymertesting.2019.03.041.

Al-Hiddabi, S.A., Pervez, T., Qamar, S.Z., Al-Jahwari, F.K., Marketz, F., Al-Houqani, S., Van de Velden, M., 2015. Analytical model of elastomer seal performance in oil wells. Appl. Math. Model. 39 (10–11), 2836–2848. https://doi.org/10.1016/j.apm.2014.10.028.

An, W.Z., Wang, Y.Y., Liu, G.H., W, C., Duan, M.L., Liu, Y.D., 2022. Study on crack fault's influence on sealing performance of metal sealing rings of subsea connectors. J. Ship Mech. 26 (1), 125–135. https://doi.org/10.3969/j.issn.1007-7294.2022.01.013.

Chen, Y., Xiao, G.P., Zhong, W.J., Yi, H., 2020. Investigation of mechanical numerical simulation and expansion experiment of expandable liner hanger in oil and gas completion. Shock Vib. 9375835. https://doi.org/10.1155/2020/9375835.

Ernens, D., Pérez-Ràfols, F., Van Hoecke, D., Roijmans, R.F.H., van Riet, E.J., Vande Voorde, J.B.E., Almqvist, A., de Rooij, M.B., Roggeband, S.M., van Haaften, W.M., Vanderschueren, M., Thibaux, P., Pasaribu, H.R., 2019. On the sealability of metal-to-metal seals with application to premium casing and tubing connections. SPE Drill. Complet. 34 (4), 382–396. https://doi.org/10.2118/194133-PA.

Gong, R., Li, X., Xu, Y., Zhang, H., 2022. Investigation of local hot spots in sealing rings with different sealing materials. Proc. IME J. J. Eng. Tribol. 236 (3), 447–459. https://doi.org/10.1177/13506501211019553.

Jiao, K.F., Yun, F.H., Hao, X.Q., Wang, G., Yao, S.M., Jia, P., Wang, X.Y., Wang, L.Q., 2024. A fast GA-ANN model and application in multi-objective optimization of the sealing ring for the subsea pipeline connector with regard of the penetration load. J. Mech. Sci. Technol. 38 (1), 309–322. https://doi.org/10.1007/s12206-023-1225-8.

Kim, G.H., Lee, Y.S., Yang, H.L., 2016. A new design concept of metal O-ring seal for long-term performance. Vacuum 123, 54–61. https://doi.org/10.1016/j.vacuum.2015.10.014.

Li, J.Y., Chang, Y.J., Xiu, Z.X., Liu, H.L., Xue, A.T., Chen, G.M., Xu, L.B., Sheng, L.X., 2020. A local stress-strain approach for fatigue damage prediction of subsea wellhead system based on semi-decoupled model. Appl. Ocean Res. 102, 102306. https://doi.org/10.1016/j.apor.2020.102306.

Li, Y.F., Jiang, W., Zeng, L., Wang, Y.Y., Liu, Z.H., Ye, S.B., 2023a. Design and characterization of subsea pipeline rehabilitation connectors. Ocean Eng. 288, 115967. https://doi.org/10.1016/j.oceaneng.2023.115967.

Li, Y.F., Su, H.L., Jiang, W., Cai, Z.Q., Chen, J.R., 2023b. Sealing performance of subsea wellhead connector under thermal-structural coupling. Ocean Eng. 270, 113504. https://doi.org/10.1016/j.oceaneng.2022.113504.

Liao, C.J., Fang, H.R., Wang, H.R., Man, M., 2017. Study on characteristics and mathematical models of stress relaxation for metal O-rings. Proc. IME J. J. Eng. Tribol. 231 (7), 826–837. https://doi.org/10.1177/1350650116682152.

Liu, W.F., Yun, F.H., Ju, M., Yao, S.M., Chen, X., 2024a2024. The reliability assessment method for sealing structure of subsea horizontal clamp connector based on sealing and strength. Ocean Eng. 311, 118938. https://doi.org/10.1016/j.oceaneng.2024.118938.

Liu, Y., Li, W.Q., Xia, C.Y., 2024b2024. Research on sealing mechanism and structural improvement of metal sealing structures for high speed drill bits. Int. J. Pres. Ves. Pip. 207, 105104. https://doi.org/10.1016/j.ijpvp.2023.105104.

Luo, X., Gu, Y., Liu, C., Qin, R., Zhao, H., Duan, M., 2014. Strength design method for tubing hanger of subsea christmas tree against big temperature difference. China Ocean Eng. 28 (5), 659–670. https://doi.org/10.1007/s13344-014-0052-1.

Meng, W.B., Fu, G.M., Huang, Y., Liu, S.J., Huang, L., Gao, Y.H., 2024. Risk assessment of deep-water horizontal X-Tree installation. China Ocean Eng. 38 (2), 210–220. https://doi.org/10.1007/s13344-024-0018-x.

Mi, L.J., An, W.Z., Chen, H.J., Han, Y.F., Sun, Q., Hou, G.X., 2023. Development mode of the shallow water subsea production system in Bohai sea area and the development status of localized equipments. China Offshore Oil Gas 35 (3), 137–146. https://doi.org/10.11935/j.issn.1673-1506.2023.03.014.

Pang, N., Jia, P., Wang, L.Q., Yun, F.H., Wang, G., Wang, X.Y., Shi, L., 2021. Dynamic Bayesian network-based reliability and safety assessment of the subsea Christmas tree. Process Saf. Environ. Prot. 145, 435–446. https://doi.org/10.1016/j.psep.2020.11.026.

Pang, N., Wang, X., Liu, Z., Xu, K., Liu, Z., Xiong, Z., Li, C., 2024. Analysis of safety and impact probability of subsea Christmas tree impacted by falling objects. Mar. Struct. 97, 103655. https://doi.org/10.1016/j.marstruc.2024.103655.

Patel, H., Salehi, S., Teodoriu, C., Ahmed, R., 2019. Performance evaluation and parametric study of elastomer seal in conventional hanger assembly. J. Petrol. Sci. Eng. 175, 246–254. https://doi.org/10.1016/j.petrol.2018.12.051.

Qiao, L.N., Keller, C., Zencker, U., Völzke, H., 2019. Three-dimensional finite element analysis of O-ring metal seals considering varying material properties and different seal diameters. Int. J. Pres. Ves. Pip. 176, 103953. https://doi.org/10.1016/j.ijpvp.2019.103953.

Qin, H., An, C., Jian, X., Duan, M.L., Ye, T.Y., Li, H., 2017. Simulation analysis of sealing performance of the K-type metal sealing ring on subsea christmas tree tubing hanger. China Offshore Oil Gas 29 (5), 141–148. https://doi.org/10.11935/j.issn.1673-1506.2017.05.020.

Saithala, J.R., Kharusi, A., Suryanarayana, M., Behlani, N., Nabhani, T., 2021. Implications of failure of alloy 718 (UNS N07718) tubing hanger in sour well. Eng. Fail. Anal. 120, 105060. https://doi.org/10.1016/j.engfailanal.2020.105060.

Wang, W.C., Yun, F.H., Sun, H., Wang, L.Q., Yan, Z.P., Wang, G., Gong, H.X., Jiao, K.F., Liu, D., Hao, X.Q., 2021. The research and experiments on contact sealing theory of the underwater clamp connector. Machines 9 (11), 262. https://doi.org/10.3390/machines9110262.

Wang, Y.Y., Luo, W.T., Liu, S.J., Feng, H.Z., Li, J.C., Wang, J.J., 2022a. A model for reliability assessment of sealing performance of the C-shaped metal sealing ring at the outlet of the subsea tubing hanger. Ocean Eng. 243, 110311. https://doi.org/10.1016/j.oceaneng.2021.110311.

Wang, Y.Y., Wang, C., Liu, G.H., Zhang, C., Li, J.C., 2022b. An assessment method of sealing performance and stress intensity factors at crack tip of subsea connector metal sealing rings. Energies 15 (13), 4680. https://doi.org/10.3390/en15134680.

Wei, Z.L., Wang, L.Q., Guan, Y., Yao, S.M., Li, S.K., 2016. Static metal sealing mechanism of a subsea pipeline mechanical connector. Adv. Mech. Eng. 8 (7). https://doi.org/10.1177/1687814016654821.

Xie, H., Zhang, H., Fan, Y., Liu, L., Zeng, W., 2025. Optimization of k-shaped metal sealing ring for subsea tubing hanger based on response surface method. Model. Simulat. Eng. 2025 (1), 1–11. https://doi.org/10.1155/mse/9995815.

Yan, H., Zhao, Y.L., Liu, J.G., Jiang, H.Y., 2016. Analyses toward factors influencing sealing clearance of a metal rubber seal and derivation of a calculation formula. Chin. J. Aeronaut. 29 (1), 292–296. https://doi.org/10.1016/j.cja.2015.09.002.

Yang, C., Cai, B.P., Wu, Q.B., Wang, C.Y.S., Ge, W.F., Hu, Z.M., Zhu, W., Zhang, L., Wang, L.T., 2023a. Digital twin-driven fault diagnosis method for composite faults by combining virtual and real data. J. Industr. Inform. Integr. 33, 100469. https://doi.org/10.1016/j.jii.2023.100469.

Yang, C., Cai, B.P., Zhang, R., Zou, Z.X., Kong, X.D., Shao, X.Y., Liu, Y.L., Shao, H.D., Khan, J.A., 2023b. Cross-validation enhanced digital twin driven fault diagnosis methodology for minor faults of subsea production control system. Mech. Syst. Signal Process. 204, 110813. https://doi.org/10.1016/j.ymssp.2023.110813.

Yun, F.H., Wang, G., Yan, Z.P., Jia, P., Xu, X.J., Wang, L.Q., Sun, H.T., Liu, W.F., 2020. Analysis of sealing and leakage performance of the subsea collet connector with lens-type sealing structure. J. Mar. Sci. Eng. 8 (6), 444. https://doi.org/10.3390/jmse8060444.

Zhang, D.W., Yang, G.C., Lv, S.C., Tian, C., Li, Z.J., 2023. Fretting behavior of static metal seal and testing apparatus for fretting friction with low/high temperature. Tribol. Int. 187, 108676. https://doi.org/10.1016/j.triboint.2023.108676.

Zhang, J., Hu, Y., 2019. Mechanical behavior and sealing performance of metal sealing system in roller cone bits. J. Mech. Sci. Technol. 33 (6), 2855–2862. https://doi.org/10.1007/s12206-019-0533-5.

Zhang, K., Cheng, H.R., Liu, J.P., Wang, H.N., 2024. Analytical calculation method for predicting contact loads and structural strength of metallic gasket of subsea connectors under thermal loads. Proc. IME M J. Eng. Marit. Environ. 238 (1), 57–67. https://doi.org/10.1177/14750902231157808.

Zhang, K., Huang, H., Duan, M.L., Hong, Y., Estefen, S.F., 2017. Theoretical investigation of the compression limits of sealing structures in complex load transferring between subsea connector components. J. Nat. Gas Sci. Eng. 44, 202–213. https://doi.org/10.1016/j.jngse.2017.03.034.

Zhang, K., Liu, J., Deng, P., Xiao, W., 2015. Sealing performance analysis of subsea Christmas tree tubing hanger. Lubr. Eng. 40 (3), 30–34. https://doi.org/10.3969/j.issn.0254-0150.2015.03.007.

Zhao, H.L., Chen, R., Luo, X.L., Duan, M.L., Lu, Y.H., Fu, G.W., Tian, H.P., Ye, D.H., 2015. Metal sealing performance of subsea X-tree wellhead connector sealer. Chin. J. Mech. Eng. 28 (3), 649–656. https://doi.org/10.3901/cjme.2015.0309.026.

Zhao, M.J., Zhu, P.C., Li, Z., Liu, Z., Kang, C., 2022. Stress analysis of self-tightness metal sealing against ultrahigh pressure medium. Strength Mater. 54 (1), 108–116. https://doi.org/10.1007/s11223-022-00390-7.

Zhao, Y.L., Yan, H., Yao, W., Jiang, H.Y., 2021. Performance degradation of metal rubber seal under high temperature and pressure. Proc. IME C J. Mech. Eng. Sci. 235 (24), 7800–7807. https://doi.org/10.1177/09544062211027611.